UWB Channel Sounding for Ranging and Positioning in Passive UHF RFID

Daniel Arnitz*, Grzegorz Adamiuk**, Ulrich Muehlmann***, and Klaus Witrisal*

* Signal Processing and Speech Communication Laboratory, Graz University of Technology, Austria
{daniel.arnitz, witrisal}@tugraz.at
** Institut für Hochfrequenztechnik und Elektronik, Karlsruher Institut für Technologie, Germany
grzegorz.adamiuk@kit.edu
*** NXP Semiconductors, Gratkorn, Austria
ulrich.muehlmann@nxp.com

***Abstract*—The market of passive UHF RFID has reached a state where it is mainly cost-driven, although there are desired features that remain elusive. Positioning, for example, has seen a lot of research in the past years, but no conclusive breakthrough. Due to limitations enforced by tag design and regulations, such positioning systems are inherently narrowband and thus vulnerable to multipath propagation. Despite that, the UHF RFID channel is not well-understood with respect to channel parameters such as K-factor or RMS delay spread, which are vital parameters for ranging accuracy.**

We present an ultra-wideband channel measurement setup aimed at the UHF RFID frequency range around 900 MHz and extending over a bandwidth of 1 GHz. Based on channel measurements in a UHF-RFID warehouse gate, we will also show the challenges positioning systems have to face in such scenarios.

***Index Terms*—UHF RFID, ultra-wideband, channel sounding, multipath propagation, warehouse portal, ranging, positioning**

I. Introduction

UHF RFID has come a long way since its early stages in the 1970s and the first standardization in the early 2000s [1]. Since then, it has become ubiquitous in various applications from supply chain management to laundry services. Even though UHF RFID is now a widespread technology, reliable positioning is a feature that is not yet available. There has been considerable research on UHF RFID positioning during the last years, but no conclusive breakthrough [2].

Foremost in the list of reasons for this are the need to keep the tag simple (power consumption, costs) and the very strict bandwidth limits of the UHF RFID frequency band(s). As a consequence, the used ranging methods are based on narrowband parameters such as return link phases and thus especially vulnerable to multipath propagation. A very good overview of such phase-based ranging and positioning systems currently under research can be found in [2].

Registering tagged objects moving through a portal is a very common application of UHF RFID [3]. The design of these gates is optimized to concentrate energy within the gate, with devastating effects on narrowband ranging systems. In this paper we present an ultra-wideband measurement setup aimed at the UHF RFID frequency range and show what challenges positioning systems have to face in everyday portal applications.

This paper is organized as follows: Section II addresses the design of the ultra-wideband (UWB) antennas that are necessary for UWB measurements in the UHF frequency range. The measurement setup is described in Section III, while the analyses methods of the measured channels is explained in detail in Section IV. Finally, measurement results are presented in Section V, including ranging error estimates for a phase-based ranging approach [4].

II. Antenna Design

A. Tag Antenna

The tag antenna (receiver-/RX-antenna in the following sections) is intended to be placed on a pallet with different goods, of which dielectric properties may vary. For that reason an antenna which preserves its properties (such as impedance matching in a wide frequency range, radiation pattern, ...), independent of the dielectric permittivity of the surroundings must be applied. Since the direction to the reader is a-priori unknown, such an antenna must maintain an omnidirectional radiation pattern.

In the presented approach a broadband dipole antenna for an operational frequency range of $0.7-1.2\,\mathrm{GHz}$ is used. The schematics of the antenna, as well as the photograph are shown in Fig. 1. It consits of two ellipses which are arranged in a dipole-like structure on the opposite sides of the substrate. As a substrate the Taconic RF-33 with $\varepsilon_r=3.3$ is used. The antenna is fed by a microstrip line, for which one of the ellipses serves as a ground plane. The connector is soldered to the microstrip line and the ground plane (cf. Fig. 1). The end of the

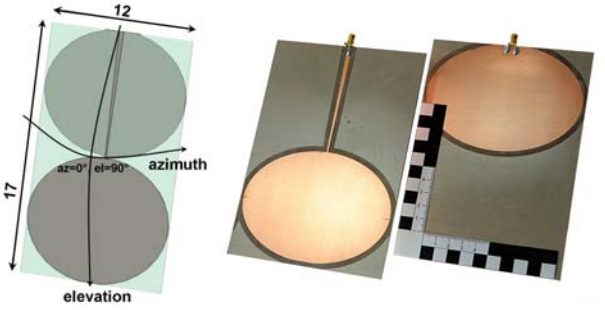

Fig. 1. Transparent model (left) and a photograph (right) of an omnidirectional tag antenna (RX). Units are in cm.

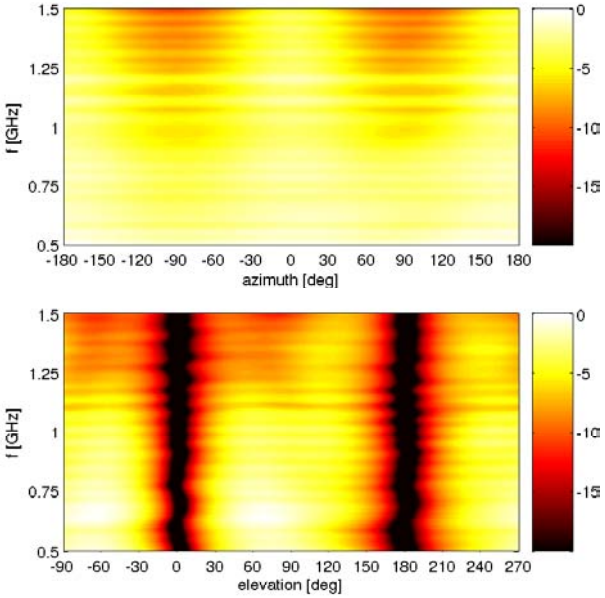

Fig. 2. Normalized horizontal/vertical gain pattern in dB: omnidirectional tag antenna.

microstrip is connected to the second ellipse. A tapering of the microstrip line's width is used for the impedance matching.

The measured gain patterns of the antenna in horizontal plane (E-plane, elevation) and vertical plane (H-plane, azimuth) are shown in Fig. 2. It can be noted that the antenna exhibits an ultra broadband radiation. In the E-plane two maxima, which are oriented perpendicular to the antenna surface, are present. In the H-plane a nearly omnidirectional radiation pattern over a wide frequency range is achieved. In the higher frequency range the antenna becomes larger w.r.t. the wavelength and some discrepancy from the omnidirectional pattern is observed. The results show that the antenna possesses a dipole-like radiation over a very wide frequency range.

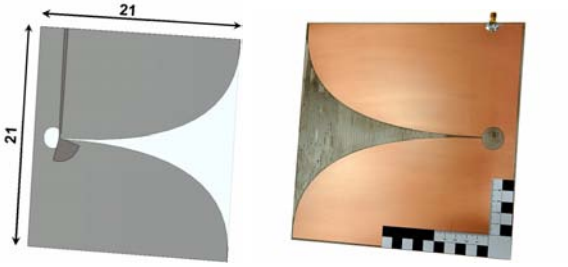

Fig. 3. Transparent model (left) and a photograph (right) of a single reader antenna. Units are in cm.

B. Reader Antenna

The reader antenna characteristics must maintain a directional radiation pattern. The operational frequency range is, as in the case of the tag antenna, from $0.7\,\text{GHz}$ to $1.2\,\text{GHz}$. An ultra-wideband radiation with directive pattern is achieved by the application of a tapered slot antenna (also called Vivaldi antenna), which is shown in Fig. 3. As a substrate the Taconic RF-30 with $\varepsilon_r{=}3$ is used. It is fed by an SMA connector, which is soldered to the microstip line at the top of the structure (see Fig. 3). The electromagnetic wave is coupled to the slot line by an aperture coupling. The slot is widened and the structure is formed to the tapered slot, which fulfils radiation conditions in a wide frequency range (according to the traveling wave principle). The lower cut-off frequency depends on the maximal opening of the slot, i.e., on the height of the antenna.

The antenna exhibits a directive radiation behavior. The main beam direction is conformal with the direction pointed by the slot opening. The $3\,\text{dB}$-beamwidth is approx. $60{-}80\,^\circ$ in the E-plane and approx. $130{-}160\,^\circ$ in the H-plane, depending on frequency. In order to assure spatial selectivity of the system in the application (e.g., a gate), the beam in the H-plane should be narrowed. For that purpose a 4×1 linear antenna array is used (transmitter-/TX-antenna in the following sections). The schematics of the antenna is shown in Fig. 4. Four Vivaldi antennas are placed next to each other in the distance of $20\,\text{cm}$. The extension plane of the array is in the H-plane of the single antenna, i.e., the horizontal plane. Such an arrangement concentrates the radiation in the respective plane and allows for the suppression of the grating lobes. The measured radiation characteristics for the elevation plane (E-plane) and the azimuth plane (H-plane) are shown in Fig. 5. A very directive radiation pattern in the azimuth plane is observed in the desired frequency range. Aside from the main beam direction, some side lobes and grating lobes are present. Their amplitude is suppressed by approx. 13 to $16\,\text{dB}$ w.r.t. the maximal gain at $0\,^\circ$. In the elevation plane a wider beam is observed. Within the main beam in this plane

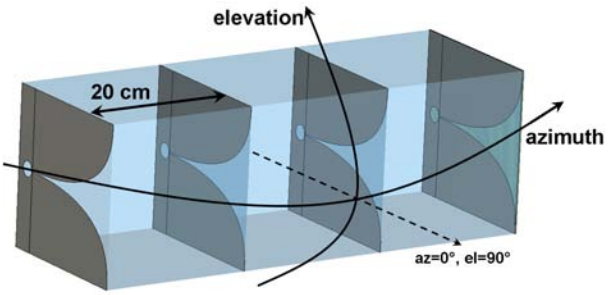

Fig. 4. Schematic of the linear 4×1 Vivaldi-array (TX).

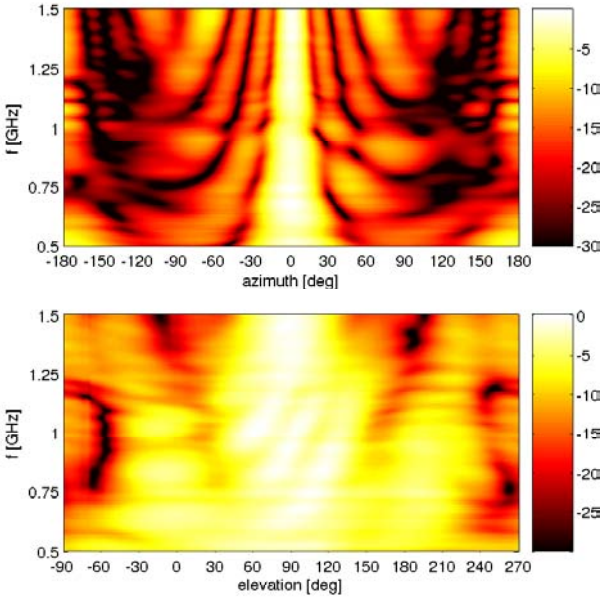

Fig. 5. Normalized horizontal/vertical gain pattern in dB: Vivaldi 4×1 array.

some small fluctuations of the gain values are present, which are due to the coupling between the elements in the array and weak resonances in the feeding network. The form of the beam in the elevation plane is conformal with the one of the single antenna.

III. Measurement Setup

A. Description of the Environment

All measurements were performed in NXP's Application and System Center (ASC) in Gratkorn, Austria, to ensure a realistic environment. The ASC is located in a converted production hall with (partially) corrugated metal walls and ceiling, and a steel-reinforced concrete floor. Among other setups, the ASC is equipped with a pallet mover that passes through several UHF RFID gates, one of which was replaced by the presented measurement setup. The entire hall is cluttered with metal objects of different sizes (from boxes with screws to a room-sized anechoic chamber).

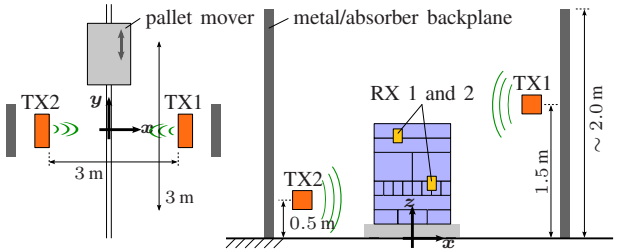

Fig. 6. Gate setup (left: top view, right: back view): A product pallet is placed on a pallet mover and transported through the gate while recording channel transfer functions (pallet was stopped for each recording).

It is also a busy environment, both physically and electrically: During the measurements, people were moving around (not within the gate), creating a time-variant and thus realistic environment. Also, as the ASC is a test center for RFID, several UHF-readers were active throughout the entire hall and cell phones were used close to the gate setup. Tests have shown that cell phones and UHF readers increase the noisefloor by approximately 20 to 30 dB for individual measurements. Even though these changes in the noisefloor are quickly time-varying due to modulation, there was no perceivable influence on the presented analyses.

B. Description of the Gate Setup

The entire setup outlined in Fig. 6 was constructed like a UHF-RFID portal: The transmitter arrays were positioned 3 m apart (front to front) to the left and right of the pallet mover. The antenna heights (floor to center) were 0.5 m (TX2) and 1.5 m (TX1), respectively. The backplanes behind the transmitter antennas (80×195 cm) are made of metal. This setup is designed to concentrate as much energy as possible within the gate and to be able to use the gate reflection to read a tag even when the direct path is blocked by the pallet. All measurements were also performed with absorber[1] backplanes of similar size to asses the influence of the metal backplanes.

Measurements with two different pallets were done: The first pallet consisted of a wooden scaffold with a polyurethane foam slab for receiver antenna mounting that was kept at a safe distance from the metal pallet mover (Fig. 7). This setup ensures wave propagation close to free space, thus forming a baseline for changes created by product pallets. The second pallet consisted of packed liquid cleaning agents in bottles, as well as some aluminum-packed candies (Fig. 8) and is considered a reference for strong distortions by NXP. A detailed schematic of this pallet (not to scale) along with receiver antenna positions can be found in Fig. 9.

[1]Emerson & Cuming ECCOSORB AN-79; reflectivity approx. -20 dB

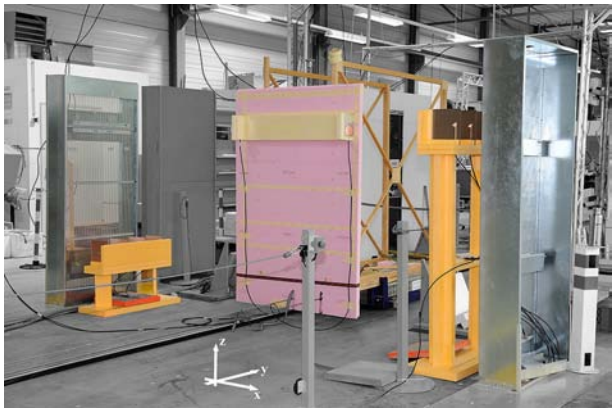

Fig. 7. Photograph of a gate setup with "free space" pallet and metal backplanes. The transmitter arrays are positioned on the stands to the left and right of the pallet mover, while the receiver antennas are mounted on the polyurethane foam slab. Note that the coordinate system is not at its origin.

Fig. 8. Photograph of a gate setup with "ETSI" pallet (liquid cleaning agents in bottles) and absorber backplanes. The receiver antennas are mounted on the polyurethane foam slab left of the pallet. Note that the coordinate system is not at its origin.

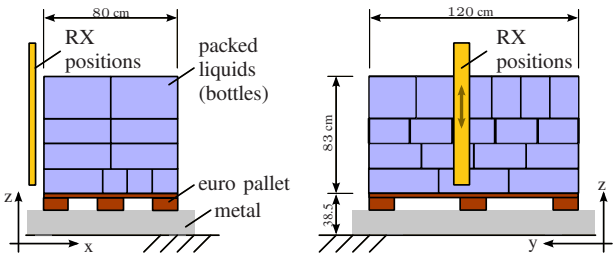

Fig. 9. Pallet with liquid cleaning agents: Back view (left) and side-view from TX2 (right). The pallet is considered a reference pallet for heavy distortions ("ETSI pallet"). A photograph can be found in Fig.8. The upper part of the receiver plane is visible to both transmitter antennas, while the lower part is visible only to TX2. Receiver antennas were kept at a distance of 10 cm from the liquids.

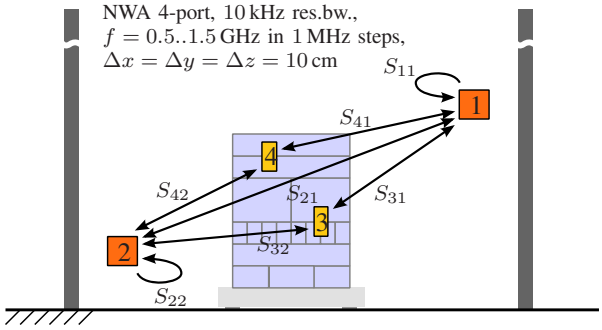

Fig. 10. Measured channels: TX at ports 1 and 2, RX at ports 1 through 4. Feedback might also be a problem for ranging systems, thus also S_{11} and S_{22} have been recorded. Shadowing properties of a product pallet and feedback for bistatic ranging setups can be analyzed via S_{21}. As tag to tag communication/ranging is not an issue in UHF RFID, receiver to receiver channels have not been recorded.

The receiver antennas were fixed at different x- and z-positions on polyurethane foam slabs, which were mounted on the pallet. The pallet was incrementally moved through the gate while recording. After each pass through the gate, the receivers were re-positioned, and the pallet was transported through the gate again. The spacing between two adjacent measurements in x, y, and z was chosen to be 10 cm to have a sufficiently high resolution within the gate while keeping the measurement time manageable. The entire set of all measurements for one receiver (lines in y) thus forms a plane in xy or yz.

All antennas were vertically polarized. Because the tag antenna gain has a minimum along this dimension, the floor reflection is considerably attenuated for some positions. It is also important to note that the cables to the receiver antennas are very critical in such setups; they have to be placed and fixed very carefully to minimize their influence on the measurement results.

The channels shown in Fig. 10 were measured for each position and in the frequency range of f=0.5..1.5 GHz with 1 MHz stepsize using a Rohde&Schwarz ZVA-24 network analyzer (NWA) with 4 ports. This stepsize results in a maximum time delay of roughly 1 μs (maximum path length 300 m), which was found to be fully sufficient in this environment. The bandwidth resolution of the NWA was 10 kHz and conducted power set to 0 dBm, resulting in a noisefloor of roughly -100 dBm and thus an effective dynamic range of 100 dB.

IV. Description of Performed Analyses

The recorded complex S-parameters for all receiver positions are analyzed as shown in Fig. 11. The individual analyses are described in detail in the following subsections.

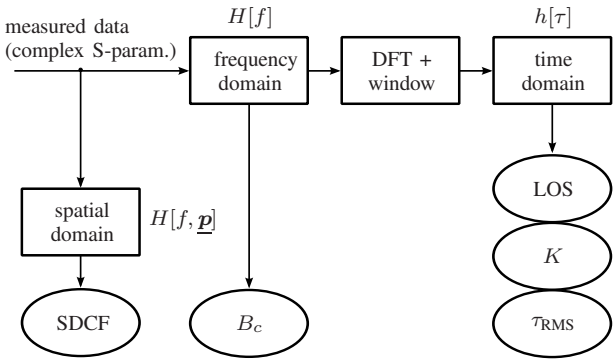

Fig. 11. Performed analyses in spatial domain, frequency domain, and time domain.

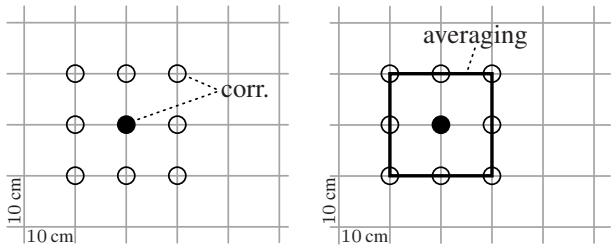

Fig. 12. Correlations in the spatial domain: The transfer function at each point is correlated with its neighbors and the resulting correlation coefficients are averaged to obtain a single coefficient.

A. Spatial Domain

Calculation of the average spaced-distance correlation function (SDCF), i.e., the correlation of the channel transfer function at each point with its nearest neighbors, is performed by averaging the correlation coefficients between the center and all its neighbors (Fig. 12). Note that this averaging neglects the inherent direction-dependence of the correlation.

B. Frequency Domain

The frequency domain analysis consist solely of calculating the coherence bandwidth B_c (cf. [5]) at several thresholds (50, 70, and 90 %). We have also implemented moment-based estimates of the K-factor [6], [7] and estimates of the RMS delay spread τ_{RMS} based on level crossing rates [7]. However, for our measurements, these estimators have been found to be unreliable due to the unknown and considerably angle-dependent (and thus position-dependent) gain patterns of the used RX and TX antennas.

C. Time-Domain

To obtain the channel impulse response (CIR) out of the channel transfer function (CTF), the spectrum is windowed by a Parzen window and transformed using a discrete Fourier transform (DFT). The CIR is subsequently truncated to remove artifacts created by cyclic convolution and re-normalized to the correct power level.

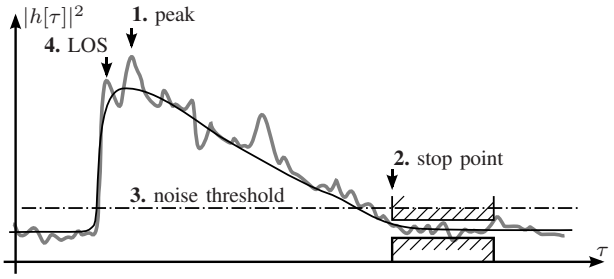

Fig. 13. Sequence of operations on the power-delay-profile: Peak detection (1), stop point detection (2), noisefloor and -threshold calculation (3), and LOS detection (4).

All calculations done for the time-domain analysis are based solely on the squared magnitude of the CIR, the power-delay-profile (PDP). The central part of the analysis is the partitioning of the PDP, as illustrated in Fig. 13: After simple peak (maximum) detection, a heavily filtered version of the PDP is created in order to detect the delay τ where the profile drops below the noisefloor (max. excess delay; denoted stop point here). To ensure a robust detection, the noisefloor is considered to be reached if the filtered version does not change by more than 3 dB for at least 200 ns. The choice of these values is arbitrary, but should reflect the shape of the PDP. As all measurements were performed in an enclosed hall without connecting corridors to other halls, clusters are not an issue. Thus, as a third step, everything after the stop point is considered noise and averaged to create the noise threshold, which is calculated using mean and standard deviation of the noise, the dispersive properties of the used window, and an additional margin of 10 dB. This margin takes the slightly higher noise level prior to the LOS component into account. The LOS path is defined to be the first component at or above this noise threshold. If the maximum peak is below the threshold, the recorded impulse response is considered noise-only. In a last step, interpolation around the detected LOS path is used to increase resolution.

Following the partitioning of the channel impulse response, several values are calculated (cf. [5]):

- LOS power and delay, taking the deformations by the used window's main lobe into account (see below)
- K-factor w.r.t. the LOS component (important for ranging) and w.r.t. the peak component ("Ricean K-factor")
- RMS delay spread with correction of the bias created by windowing (see below)

It is of vital importance here to consider the effects of the used window on all calculations: Not only will the window's main lobe broaden the LOS peak (if there is a peak in the first place), but the strongest sidelobe

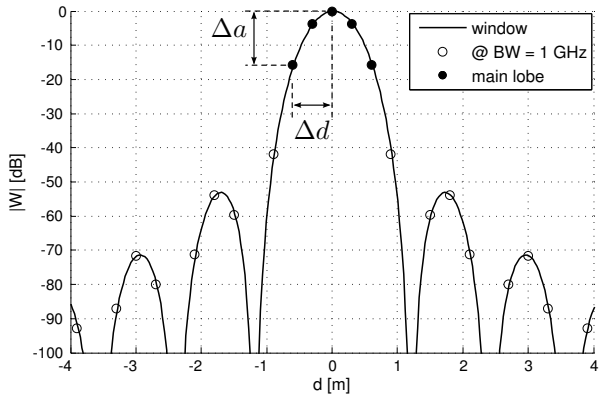

Fig. 14. Used Parzen window (circles): Max. mainlobe attenuation Δa, mainlobe width $2\Delta d$. The considered mainlobe for the presented measurements consists of 5 points, hence $> 99.99\,\%$ of the window power is within the main lobe.

will also shift energy from the possibly very strong LOS peak to the noisefloor that precedes the LOS path. If this sidelobe is sufficiently pronounced and not considered in the threshold calculation, the artifact will be identified as LOS component. These distortions introduced by windowing are factored in at four different points (cf. Fig. 14):

1) The noise threshold is increased by the gain difference of minimum and maximum mainlobe sample (Δa).
2) The true LOS position is assumed to be close to Δd after the threshold crossing.
3) For K-factor calculations, ± 2 samples around the LOS position are considered to be part of the LOS component.
4) The bias for the RMS delay spread created by windowing [8] is corrected. It should be noted though that this bias is merely 0.75 ns for the used Parzen window.

V. Measurement Results

For the sake of brevity, the majority of measurement results shown here are limited to the most realistic setup: The gate with metal backplanes and the liquids ("ETSI") pallet. As mentioned above, this pallet is considered a reference and is thus also a good benchmark for ranging and positioning. Photograph and schematic of the setup can be found in Figs. 8 and 9, respectively.

We will start our analysis with the incident power level at the tag. This is the single most important value for the analysis of state-of-the-art UHF RFID systems, as it is directly connected to read rates and thus to the most important performance metric for RFID users. A comprehensive analysis of the incident power distribution in a portal application can be found in [3]. The

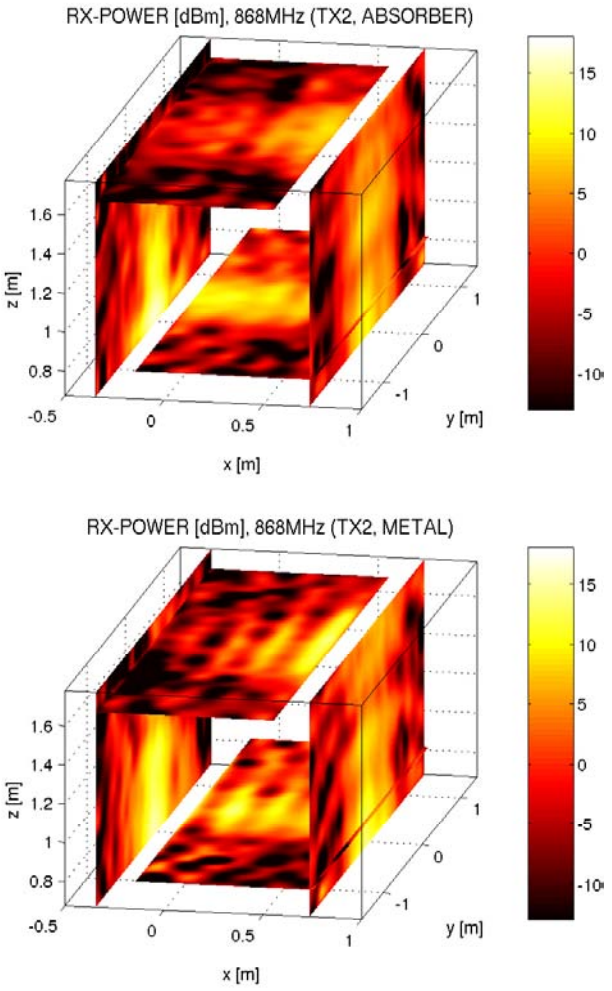

Fig. 15. Incident power level [dBm] at the tag for 35.2 dBm (EIRP) conducted power at 868 MHz and TX2; empty gate with absorber/metal backplanes

circular line structure created by standing waves within the empty gate predicted by simulations in [3] and [9] can also be observed here: Fig. 15 shows some vertical circles created by the floor reflection for the absorber backplanes, as well as pronounced standing waves in horizontal and vertical planes for the metal backplanes.

Things change considerably when a pallet enters the gate: Fig. 16 shows the power distribution for TX1 and TX2. The standing wave pattern is destroyed by the moving pallet (which is highly reflective itself). A slight circular structure (created by the floor reflection) can be observed after the pallet has left the gate ($y > 1$ m).

Even though the incident power level at a certain frequency is a vital metric for UHF RFID, its importance to ranging and positioning is minimal. On the other hand, the K-factor w.r.t. the direct (LOS) path and the RMS delay spread are of paramount importance here, and shown for the liquids pallet in Figs. 17 and 18,

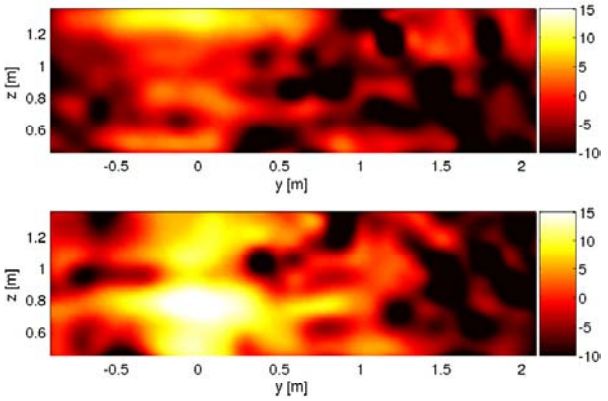

Fig. 16. Incident power level [dBm] at the tag; 35.2 dBm (EIRP) conducted power at 868 MHz; TX1 (top) and TX2 (bottom); "ETSI pallet", metal backplanes; view from TX1.

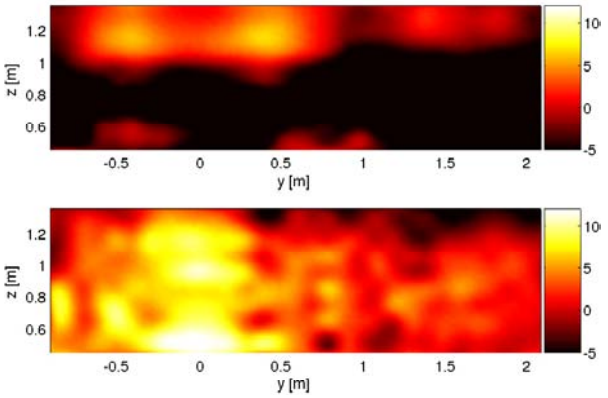

Fig. 17. K-Factor [dB] w.r.t. the LOS component for TX1 (top) and TX2 (bottom); "ETSI pallet", metal backplanes; view from TX1.

respectively. Considering the reflective properties of the used materials (metal backplanes, a metal pallet mover, a steel-reinforced concrete floor, and a cubic meter of liquids), it comes at no surprise that the K-factor only exceeds $K \approx 5\,\mathrm{dB}$ when the receiver is directly in front of the transmitter array ($y = -30..30\,\mathrm{cm}$). Still, considering that the distance to the array in this case is less than one meter, K-factors are surprisingly low. The same is true for the RMS delay spread, which is above 10 ns for almost the entire gate. For comparison, this delay of 10 ns corresponds to a path length of 3 m in free space.

Fig. 19 shows a comparison of the K-factor w.r.t. the direct path for metal and absorber backplanes. As can be seen, the K-factor inside the gate drops considerably for the metal backplanes.

The coherence bandwidth (correlation in frequency domain) is shown in Fig. 20, while the spaced-distance correlation function (correlation in spatial domain) can be found in Fig. 21. As can be seen, the 90 % coher-

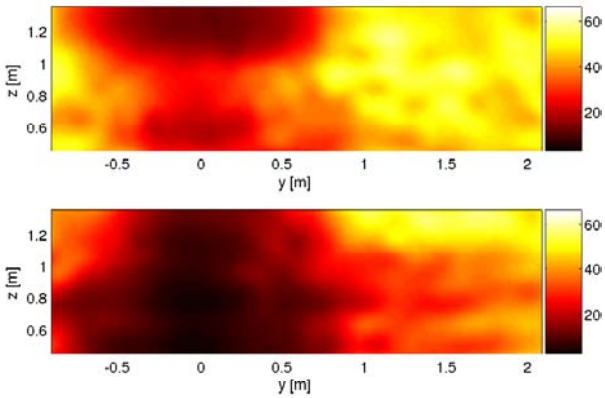

Fig. 18. RMS delay spread [ns] for TX1 (top) and TX2 (bottom); "ETSI pallet", metal backplanes; view from TX1.

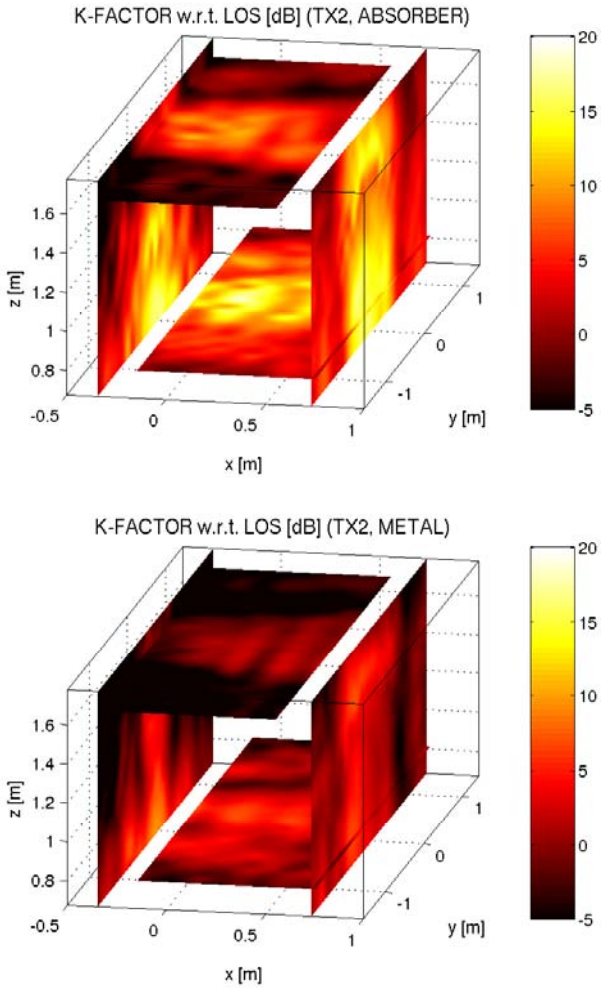

Fig. 19. K-Factor [dB] w.r.t. the LOS component for TX2; empty gate with absorber/metal backplanes

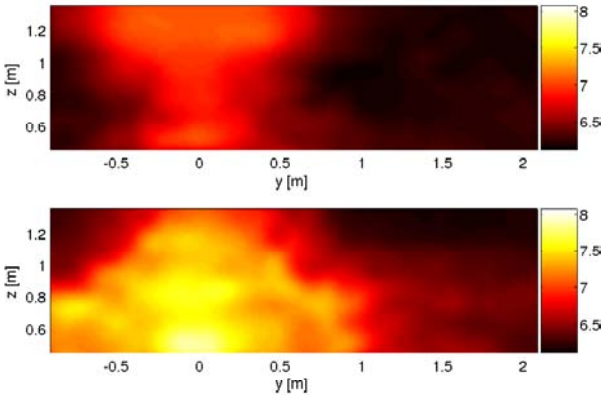

Fig. 20. 90 % coherence bandwidth [log10(Hz)] for TX1 (top) and TX2 (bottom); "ETSI pallet", metal backplanes; view from TX1.

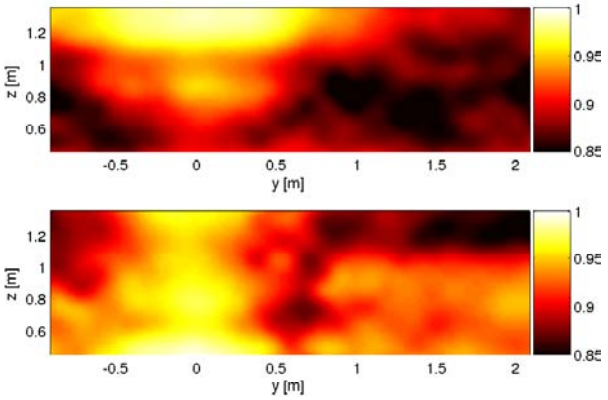

Fig. 21. Spaced-distance correlation function at $\Delta = 12\,\mathrm{cm}$ for TX1 (top) and TX2 (bottom); "ETSI pallet", metal backplanes; view from TX1.

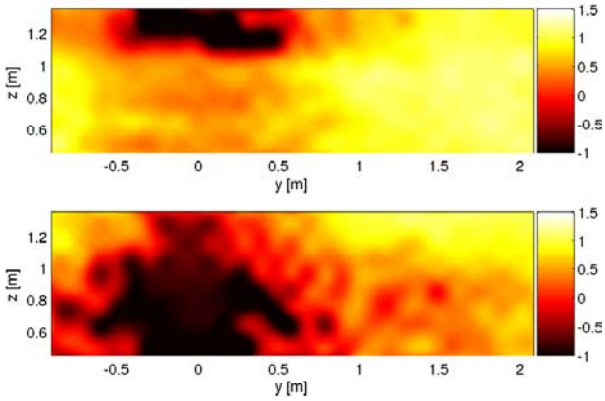

Fig. 22. Expected value (bias) log10([m]) of a single 2FCW estimate w. $\Delta f = 1\,\mathrm{MHz}$ for TX1 (top) and TX2 (bottom); "ETSI pallet", metal backplanes; view from TX1.

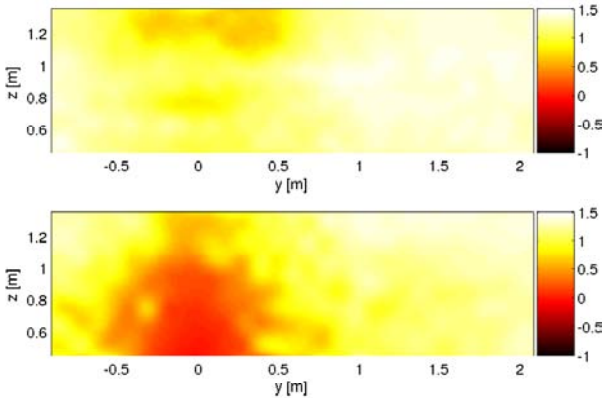

Fig. 23. Standard deviation log10([m]) of a single 2FCW estimate w. $\Delta f = 1\,\mathrm{MHz}$ for TX1 (top) and TX2 (bottom); "ETSI pallet", metal backplanes; view from TX1.

ence bandwidth is in the range of $50\,\mathrm{MHz}$ inside the gate when in direct line of sight, and around $1\,\mathrm{MHz}$ outside the gate. Correlations at a length (distance) of $12\,\mathrm{cm}$, which is $20..60\,\%$ of a wavelength for the given frequency range, are above $90\,\%$ for most of the gate. The estimated coherence length ($70\,\%$) is around $1..2$ wavelengths outside the gate, if the direct path is blocked by the pallet, and several wavelengths inside the gate. Curiously, the coherence distance is almost independent of the used backplane.

Last, but not least, the error for a phase-based ranging method [4] with a frequency spacing of $1\,\mathrm{MHz}$ is shown in Figs. 22 and 23. Note that these are the errors for the path TX→RX and a single ranging estimate.

Fig. 22 shows the expected value (bias) of this estimate. Outside the gate, the combined non-line-of-sight (NLOS) paths are stronger than the direct LOS path by far, leading to a heavily biased estimate. Said bias ranges from below $10\,\mathrm{cm}$ inside the gate provided the LOS path is not blocked by the pallet, and reaches up to $20\,\mathrm{m}$ outside the gate. The standard deviation for a single estimate (Fig. 23) ranges from roughly $1.5\,\mathrm{m}$ in front of the transmitter (at a distance of less than a meter!) to $30\,\mathrm{m}$ outside the gate. Note that the wavelength of the offset frequency ($1\,\mathrm{MHz}$) is $300\,\mathrm{m}$; thus the phase difference is still non-ambiguous. As the standard deviation can be reduced by successive/independent range estimates, classification "inside/outside gate" still might be possible. In fact, the bias will help for such a classification, as it will quickly shift the range estimate to outside the gate (note the almost linearly increasing bias in this logarithmic plot).

VI. Conclusion

We have presented a measurement setup for channel sounding in the UHF RFID frequency band. Using this setup, we have done extensive measurements in a UHF RFID portal scenario under realistic conditions. The presented measurements are widely consistent with

previous measurements in this portal [3] in terms of narrowband power levels.

The design of UHF RFID portals is optimized for best possible read rates, employing metal backplanes to concentrate energy within the portal. This design has devastating effects on narrowband ranging systems, as it reduces K-factors w.r.t. the LOS component by more than 10 dB and increases the RMS delay spread by factors. Is should also be noted that the channel inside such a portal is highly deterministic [2], [3]. Any ranging system has to deal with K-factors w.r.t. the direct path in the range of 5..10 dB at best, and RMS delay spreads above 10 ns even at distances below one meter.

RMS delay spreads outside the gate (but still with an unobstructed direct path) reached 60 ns in our measurements, while K-factors dropped well below 0 dB. In this aspect our results correspond well with measurements at distances up to 20 m in an industrial environment [10]. It follows that the exterior of the gate, i.e., everything outside the space spanned by the metal backplanes, has to be treated as non-line-of-sight, even if the direct path is unobstructed. Furthermore, we find that previous short-range measurements in the UHF band [8] and other short-range channel models like IEEE 802.15.3a [11] (based on meas. [12], [13]) are too optimistic for UHF RFID gates even when considering the worst case scenario of these models.

VII. Acknowledgments

The authors would like to thank NXP Semiconductors, Gratkorn, Austria, for funding this project and for providing the environment for all measurements. We would also like to thank Giuliano Manzi, Gerald Wiednig, Martin Rampetsreiter, and Alexey Nazarov for manufacturing all used antennas and for their help with the measurement setup, as well as Albert Angstenberger from Taconic for providing the substrate for the antennas. This work was supported by the Austrian Research Promotion Agency (FFG) under the grant number 818072.

References

[1] D. M. Dobkin, *The RF in RFID*. Elsevier, 2007, ISBN-13: 978-0750682091.

[2] P. V. Nikitin, R. Martinez, S. Ramamurthy, H. Leland, G. Spiess, and K. V. S. Rao, "Phase based spatial identification of UHF RFID tags," in *Proc. IEEE Int RFID Conf*, 2010, pp. 102–109.

[3] U. Muehlmann, G. Manzi, G. Wiednig, and M. Buchmann, "Modeling and performance characterization of UHF RFID portal applications," *IEEE Trans. Microw. Theory Tech.*, vol. 57, no. 7, pp. 1700–1706, 2009.

[4] D. Arnitz, K. Witrisal, and U. Muehlmann, "Multi-frequency continuous-wave radar approach to ranging in passive UHF RFID," *IEEE Trans. Microw. Theory Tech.*, vol. 57, no. 5, pp. 1398–1405, Jul. 2009.

[5] A. Molisch, *Wireless Communications*, 1st ed. John Wiley & Sons, 2005, ISBN-13: 978-0470848876.

[6] C. Tepedelenlioglu, A. Abdi, and G. B. Giannakis, "The ricean K factor: estimation and performance analysis," *IEEE Trans. Wireless Commun.*, vol. 2, no. 4, pp. 799–810, 2003.

[7] K. Witrisal, Y.-H. Kim, and R. Prasad, "A new method to measure parameters of frequency-selective radio channels using power measurements," *IEEE Trans. Commun.*, vol. 49, no. 10, pp. 1788–1800, Oct. 2001, 10.1109/26.957401.

[8] M. S. Varela and M. G. Sánchez, "RMS delay and coherence bandwidth measurements in indoor radio channels in the UHF band," *IEEE Trans. Veh. Technol.*, vol. 50, no. 2, pp. 515–525, Mar. 2001, 10.1109/25.923063.

[9] G. Marrocco, E. Di Giampaolo, and R. Aliberti, "Estimation of UHF RFID reading regions in real environments," *IEEE Antennas Propag. Mag.*, vol. 51, no. 6, pp. 44–57, 2009.

[10] T. Gigl, T. Buchgraber, A. Adalan, J. Preishuber-Pfluegl, M. Fischer, and K. Witrisal, "UWB channel characterization using IEEE 802.15.4a demonstrator system," in *Proc. IEEE Int. Conf. Ultra-Wideband ICUWB 2009*, 2009, pp. 230–234.

[11] A. F. Molisch, J. R. Foerster, and M. Pendergrass, "Channel models for ultrawideband personal area networks," *IEEE Wireless Commun. Mag.*, vol. 10, no. 6, pp. 14–21, 2003.

[12] J. R. Foerster and Q. Li, "UWB channel modeling contribution from intel," IEEE Tech. Rep. P802.15 02/279SG3a, 2002, IEEE P802.15 SG3a Contribution.

[13] M. Pendergrass and W. Beeler, "Empirically based statistical ultra-wideband (UWB) channel model," IEEE Tech. Rep. P802.15 02/240SG3a, 2002, IEEE P802.15 SG3a Contribution.